Chapter 6

Experimental and Numerical Study of an Optoelectronics Flexible Logic Gate Using a Chaotic Doped Fiber Laser

Juan Hugo García-López, Rider Jaimes-Reátegui, Samuel Mardoqueo Afanador-Delgado, Ricardo Sevilla-Escoboza, Guillermo Huerta-Cuéllar, Didier López-Mancilla, Roger Chiu-Zarate, Carlos Eduardo Castañeda-Hernández and Alexander Nikolaevich Pisarchik

Additional information is available at the end of the chapter

http://dx.doi.org/10.5772/intechopen.75466

Abstract

In this chapter, we present the experimental and numerical study of an optoelectronics flexible logic gate using a chaotic erbium-doped fiber laser. The implementation consists of three elements: a chaotic erbium-doped fiber laser, a threshold controller, and the logic gate output. The output signal of the fiber laser is sent to the logic gate input as the threshold controller. Then, the threshold controller output signal is sent to the input of the logic gate and fed back to the fiber laser to control its dynamics. The logic gate output consists of a difference amplifier, which compares the signals sent by the threshold controller and the fiber laser, resulting in the logic output, which depends on an accessible parameter of the threshold controller. The dynamic logic gate using the fiber laser exhibits high ability in changing the logic gate type by modifying the threshold control parameter.

Keywords: optical logic devices, optoelectronics, fiber laser, chaos

1. Introduction

An important advantage of erbium-doped fiber lasers (EDFLs) over other optical devices is a long interaction length of the pumping light with active ions that leads to a high gain and a single transversal-mode operation for a suitable choice of fiber parameters. The EDFL with coherent radiation at the wavelength of 1560 nm is an excellent device for applications in medicine, remote sensing, reflectometry, and all-optical fiber communications networks [1, 2]. Rare-doped fiber lasers subjected to external modulation from semiconductor pump lasers are known to exhibit chaotic dynamics [3–12]. Besides, a very important advantage of the EDFL working in a chaotic regimen is its application to the development of basic logic gates [13], since it can process different logical gates and implements diverse arithmetic operations. The simplicity in switching chaotic EDFL between different logical operations makes this device more suitable for general proposes than traditional computer architecture with fixed wire hardware.

Using a chaotic system as a computing device was proposed by Sinha and Ditto [14], who applied for this purpose a chaotic Chua's circuit with a simple threshold mechanism. After this pioneering work, chaotic computational elements received considerable attention from many researchers who developed new designs allowing higher capacity for universal general computing purposes enable to reproduce basic logic operations, such as AND, OR, NOT, XOR, NAND, and NOR [15–26]. Likewise, a single chaotic element has the ability in reconfiguring into different logic gates through a threshold-based control [15, 16]. This device is also known as reconfigurable chaotic logic gate (RCLGs) and, due to its inherent nonlinear components, has advantages over standard programmable gate array elements [19] where reconfiguration is obtained by interchanging between multiple single-purpose gates. Also, discrete circuits working as RCLGs were proposed to reconfigure all logic gates [17, 18]. Additionally, reconfigurable chaotic logic gates arrays (RCGA), which morph between higher-order functions, such as those found in a typical arithmetic logic unit (ALU), were invented [20]. Recently, some of the authors of this work proposed an optoelectronics flexible logic gate based on a fiber laser [27, 28].

Here, we describe in detail the implementation of the optoelectronics flexible logic gate based on EDFL, which exploits the richness and complexity inherent to chaotic dynamics. Using a threshold controller, NOR and NAND logic operations are realized in the chaotic EDFL.

This chapter is an extension of the article "*Optoelectronic flexible logic gate based on a fiber laser. Eur. Phys. J. Special Topics. 2014*" [27]. It is organized as follows. The theoretical model of the diode-pumped EDFL is described in Section 2. The experimental setup of the optical logic gate based on the EDFL is given in Section 3. Likewise, the discussion of theoretical and experimental results on the application of the NAND and NOR logic gates based on the EDFL as a function of the threshold controller is presented in Section 4. Finally, main conclusions are given in Section 5.

2. Theoretical arrangement

The EDFL is known to be extremely sensitive to external disturbances, which can destabilize its normal operation. This makes this device very promising for many applications where small-amplitude external modulation is required to control the laser dynamics. The mathematical

http://dx.doi.org/10.5772/intechopen.75466

model and experimental arrangement of the EDFL used in this work have been developed by Pisarchik et al. [6–12].

2.1. EDFL theoretical model

Based on the power balance approach, we model diode-pumped EDFL dynamics by considering both the excited-state absorption (ESA) in erbium at the 1560-nm wavelength and the averaged population inversion along the pumped active fiber laser. The model addresses two evident factors, the ESA at the laser wavelength and the depleting of the pump wave at propagation along the active fiber, leading to undumped oscillations experimentally observed in the EDFL without external modulation [6, 12]. The energy-level diagram of the theoretical model used in this work is shown in **Figure 1**.

Using a conventional system for EDFL balance Equations [6, 7], which describe the variations of the intra-cavity laser power P (in units of s^{-1}), that is, the sum of the contrapropagating waves' powers inside the cavity and the averaged population N (dimensionless variable) in the upper laser level "2," we can write EDFL equations as follows:

$$\frac{dP}{dt} = \frac{2L}{T_r} P[r_\omega \alpha_0 (N[\xi - \eta] - 1) - \alpha_{th}] + P_{sp} \tag{1}$$

$$\frac{dN}{dt} = -\frac{\sigma_{12} r_\omega P}{\pi r_0^2}(\xi N - 1) - \frac{N}{\tau} + P_{pump} \tag{2}$$

where N can take values between $0 \leq N \leq 1$ and is defined as $N = \frac{1}{n_0} L \int_0^L N_2(z)\, dz$, with N_2 as the upper laser-level population density "2," n_0 is the refractive index of an erbium-doped fiber, and L is the length of the active fiber medium; σ_{12} is the cross section of the absorption transition from the state "1" to the upper state "2," σ_{12} is the stimulated cross section of the transition in return from the upper state "2" to the ground state "1," in

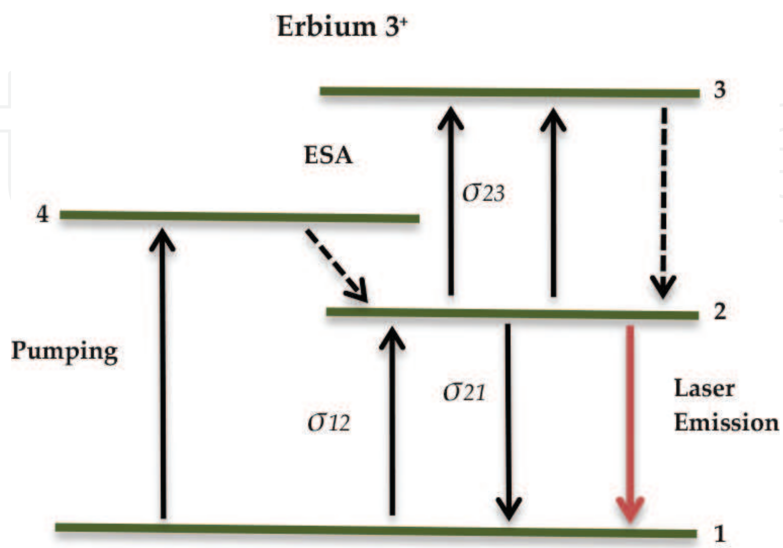

Figure 1. Erbium-doped fiber laser energy diagram.

magnitude practically are the same, that is, $\sigma_{21} = \sigma_{12}$, that gives $\xi = \frac{\sigma_{12}+\sigma_{21}}{\sigma_{12}} = 2$; $\eta = \frac{\sigma_{23}}{\sigma_{12}}$ is the coefficient ratio between excited-state absorption (σ_{23}) and the ground-state absorption cross sections (σ_{12}); $\tau_r = \frac{2n_0(L+l_0)}{c}$ is the photon round-trip time in the cavity (l_0 is the length intra-cavity tails of FBG couplers); $\alpha_0 = N_0\sigma_{12}$ is the small-signal absorption of the erbium fiber at the laser wavelength ($N_0 = N_1 + N_2$ is the total erbium ions' populations density in the active fiber medium); $\alpha_{th} = \gamma_0 + \frac{ln(1/R_B)}{2L}$ is the cavity losses at threshold (γ_0 being the passive fiber losses, R_B is the total reflection coefficient of the fiber Bragg grating (FBG) couplers); τ is the lifetime of erbium ions in the excited state "2"; r_ω is the factor addressing a match between the laser fundamental mode and erbium doped core volumes inside the active fiber, given as

$$r_\omega = 1 - \exp\left[-2\left({}^{r_0}/_{\omega_0}\right)^2\right], \tag{3}$$

where r_0 is the fiber core radius and w_0 is the radius fundamental fiber mode. The spontaneous emission P_{sp} into the fundamental laser mode is taken as

$$P_{sp} = \frac{y10^{-3}}{\tau T_\tau}\left(\frac{\lambda_g}{\omega_0}\right)^2 \frac{r_0^2\alpha_0 L}{4\pi^2\sigma_{12}}. \tag{4}$$

Here, we assume that the erbium luminescence spectral bandwidth (λ_g being the laser wavelength) is 10^{-3}. P_{pump} is the laser pump power given as

$$P_{pump} = P_P \frac{1 - \exp\left[-\beta\alpha_0 L(1-N)\right]}{n_0\pi r_0^2 L}, \tag{5}$$

where P_p is the pump power at the fiber entrance and $\beta = \frac{\alpha_p}{\alpha_0}$ is the dimensionless coefficient that accounts for the ratio of absorption coefficients of the erbium fiber at pump wavelength λ_p to that at laser wavelength λ_g. Eqs. (1) and (2) describe the laser dynamics without external modulation. We add the modulation to the pump parameter as:

$$P_{pump} = P_p^0[1 + A_m \sin(2\pi F_m t)], \tag{6}$$

where P_p^0 is the laser pump power without modulation, A_m and F_m are the modulation amplitude and frequency, respectively.

We perform numerical simulations for the laser parameters corresponding to the following experimental conditions from references [6, 7]: L = 90 cm, n_0 = 1.45 and l_0 = 20 cm, giving T_r = 8.7 ns, $r_0 = 1.5 \times 10^{-4}$ cm, and $w_0 = 3.5 \times 10^{-4}$ cm. The value of w_0 is measured experimentally and using Eq. (3) resulting in r_w = 0.308. The coefficients characterizing the resonant-absorption properties of the erbium fiber at the laser and pump wavelengths are α_0 = 0.4 cm^{-1} and β = 0.5 (corresponding to direct measurements for doped fiber with erbium concentration of 2300 ppm); $\sigma_{12} = \sigma_{21} = 3 \times 10^{-21}$ cm^2 and $\sigma_{23} = 0.6 \times 10^{-21}$ cm^2 giving $\xi = 2$ and η = 0.2; $\tau = 10^{-2}$ s [6, 7]; γ_0 = 0.038 and R_B = 0.8 with a cavity losses at threshold of

http://dx.doi.org/10.5772/intechopen.75466

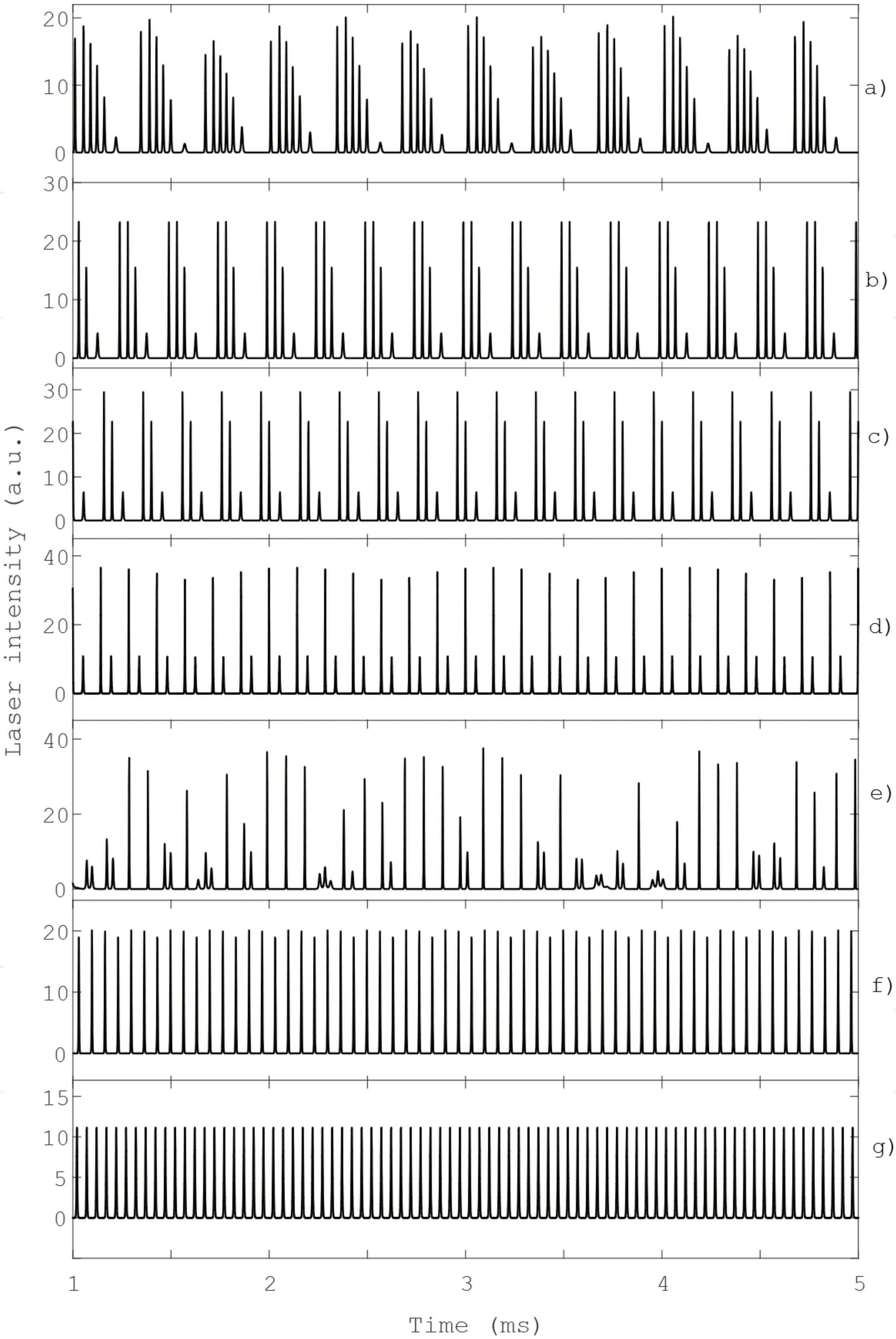

Figure 2. Time series of laser intensity P, with $A_m = 1$, and (a) $F_m = 3$ kHz, (b) $F_m = 4$ kHz, (c) $F_m = 3$ kHz, (d) $F_m = 7$ kHz, (e) $F_m = 10$ kHz, (f) $F_m = 15$ kHz, and (g) $F_m = 20$ kHz.

α_{th} = 3.92 × 10^{-2}. The laser wavelength is λ_g = 1.56 × 10^{-4} cm (photon energy hv_g = 1.274 × 10^{-19} *J*) corresponding to the maximum reflection coefficients of both FBG's.

The laser threshold is defined as $\varepsilon = P_p/P_{th}$, where

$$P_{th} = \frac{N_{th}}{\tau} \frac{n_0 \pi r \omega_p^2 L}{1 - \exp[-\beta \alpha_0 L(1 - y_{th})]} \tag{7}$$

is the threshold pump power, $N_{th} = \frac{1}{\xi}\left(1 + \frac{\alpha_{th}}{r_\omega \alpha_0}\right)$ is threshold population of the level "2" and the radius of the pump beam $w_p = w_0$. In the numerical simulations, we choose the pump power P_p = 7.4 × 10^{19} s^{-1} that yields the laser relaxation oscillation frequency $f_0 \approx$ 30 kHz.

In order to understand the dynamics of the EDFL, the bifurcation diagram of the local maxima of the laser power versus the pump modulation frequency F_m is calculated. To perform numerical simulations, we normalize Eqs. (1) and (2) (as described in the appendix of reference [29]) and obtain the following equations:

$$\frac{dx}{dt} = axy - bx + c(y + r_\omega), \tag{8}$$

$$\frac{dy}{dt} = -dxy - (y + r_\omega) + e\left\{1 - exp\left[-\beta \alpha_0 L\left(1 - \frac{N_2 + r_\omega}{\xi_2 r_\omega}\right)\right]\right\}, \tag{9}$$

Figure 2 presents the time series of the laser intensity at the following driven frequencies: (a) F_m = 3 kHz, the laser behavior is chaotic, (b) F_m = 4 kHz, the EDFL response is a period 4, (c) F_m = 3 kHz, the EDFL response is a period 3, (d) F_m = 7 kHz, the EDFL response is a period 2, (e) F_m = 10 KHz, chaos, (f) F_m = 15 kHz and (g) F_m = 20 kHz, a period 1 with decreasing amplitude as the modulation frequency is increased.

The constant parameters of Eqs. (8) and (9) are shown in **Table 1** [30].

Figure 3 shows the numerical bifurcation diagram of the laser peak intensity versus the modulation frequency (0–20 kHz) for the 100% modulation depth (A_m = 1). The laser dynamical behavior (periodic or chaotic) is determined by the modulation frequency.

In this work, we are interested in a chaotic regime. **Figure 4** shows the times series corresponding to chaos for F_m = 10 kHz.

Constant parameter	Values (a.u.)
a	6.6207 × 10^7
b	7.4151 × 10^6
c	0.0163
d	4.0763 × 10^3
e	506

Table 1. Normalized constant parameters of Eqs. (8) and (9).

http://dx.doi.org/10.5772/intechopen.75466

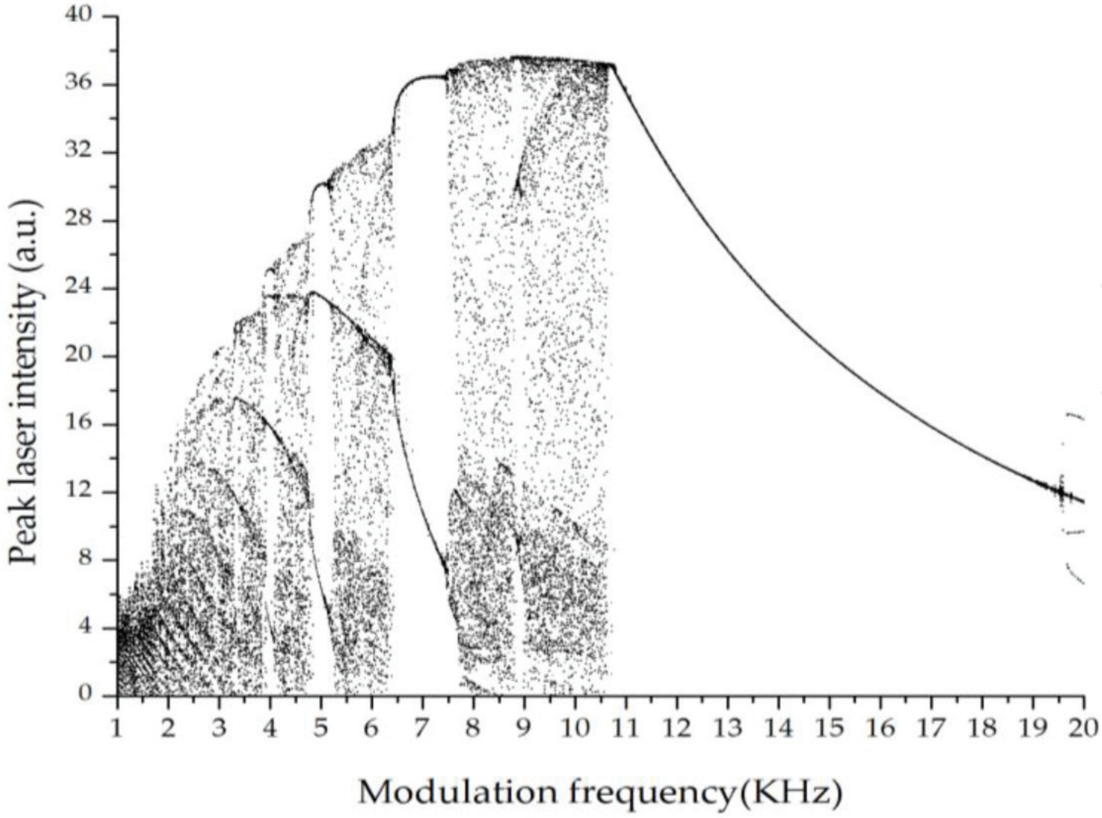

Figure 3. Numerical bifurcation diagram of laser peak intensity versus modulation frequency (F_m) for A_m = 1.

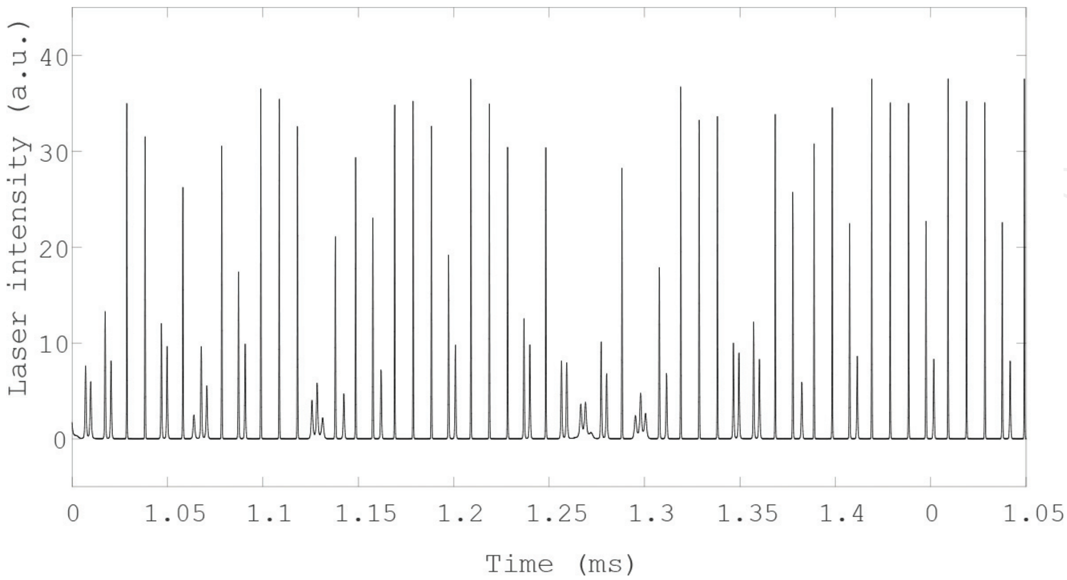

Figure 4. Time series of laser intensity P for F_m = 10 kHz and A_m = 1.

3. Implementation of the optoelectronics flexible logic gate using the EDFL

Figure 5 shows the scheme of the proposed optoelectronics flexible logic gate using the EDFL. The reconfigurable logical gate contains two principal elements: a chaotic EDFL and a threshold controller. The dynamics behavior of the EDFL is described by the balance Eqs. (1) and (2). The threshold controller compares laser power P with value V_T generated by the controller that releases output $V_T = E$ if $P > E$ and $V_T = P$ otherwise, with E as threshold value. This output signal V_T is added to the diode pump current P_{pump} with a coupling coefficient K. The logic gate output subtracts V_T from P yielding $V_0 = P - V_T$. Next, we consider the laser and the controller models separately.

3.1. Threshold controller

In our numerical simulations, we use the laser power P calculated by Eqs. (1), (2), and (6) as the input signal for the threshold controller. The output signal V_T from the controller is used to control the diode pump current as:

$$P_{pump} = P_p[1 + A_m \sin(2\pi F_m t) + KV_T] \tag{10}$$

The threshold controller has two logic inputs 0 and 1, which generate the corresponding values I_1 and I_2, where $I_{1,2} = 0$ for input 0 and $I_{1,2} = V_{in}$ otherwise, where V_{in} is a certain value to define the threshold for E. A type of the logic gate is determined by a parameter V_c. The procedure to obtain this parameter is explained in detail in section Results and Discussions.

The controller generates an initial value E defined by the inputs I_1 and I_2 being either 0 or V_{in} and takes the value:

$$E = V_c + I_1 + I_2 \tag{11}$$

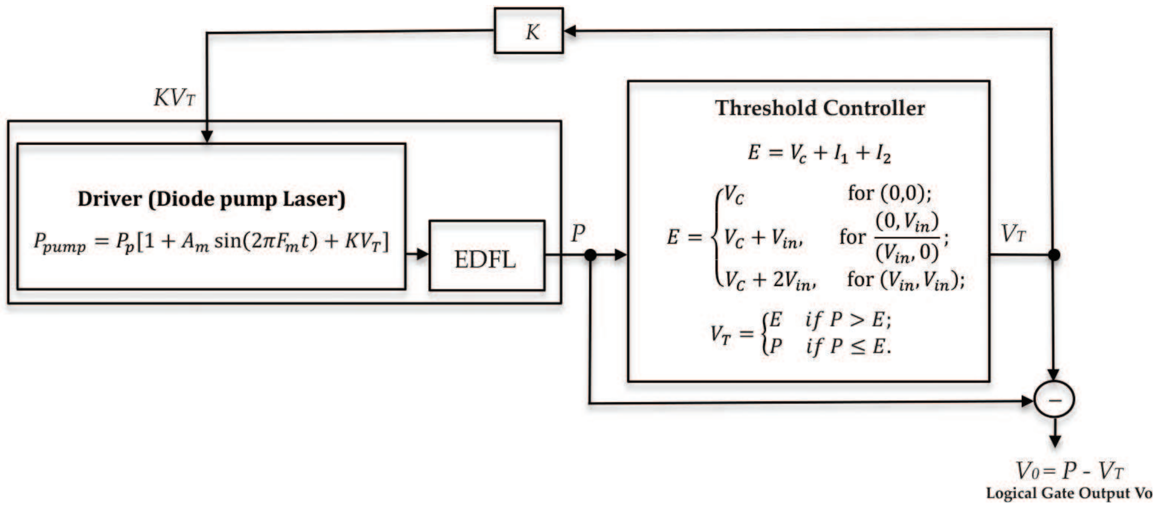

Figure 5. Arrangement of the optoelectronics logic gate. E is the threshold controller, V_c determines the logic response, $I_{1,2}$ is the logic input which takes the value of either V_{in} or 0, V_T is the output controller signal, P is the laser output intensity, P_{pump} is the diode laser pump intensity, P_p is the continuous component of the pumping, A_m and F_m are the modulation depth and frequency, and K is the gain factor.

so that there are three possible options:

$$E = \begin{cases} V_C & \text{for } (0,0), \\ V_C + V_{in}, & \text{for } \dfrac{(0, V_{in})}{(V_{in}, 0)}, \\ V_C + 2V_{in}, & \text{for } (V_{in}, V_{in}). \end{cases} \tag{12}$$

The controller output is determined as:

$$V_T = \begin{cases} E & \text{if } P > E, \\ P & \text{if } P \leq E. \end{cases} \tag{13}$$

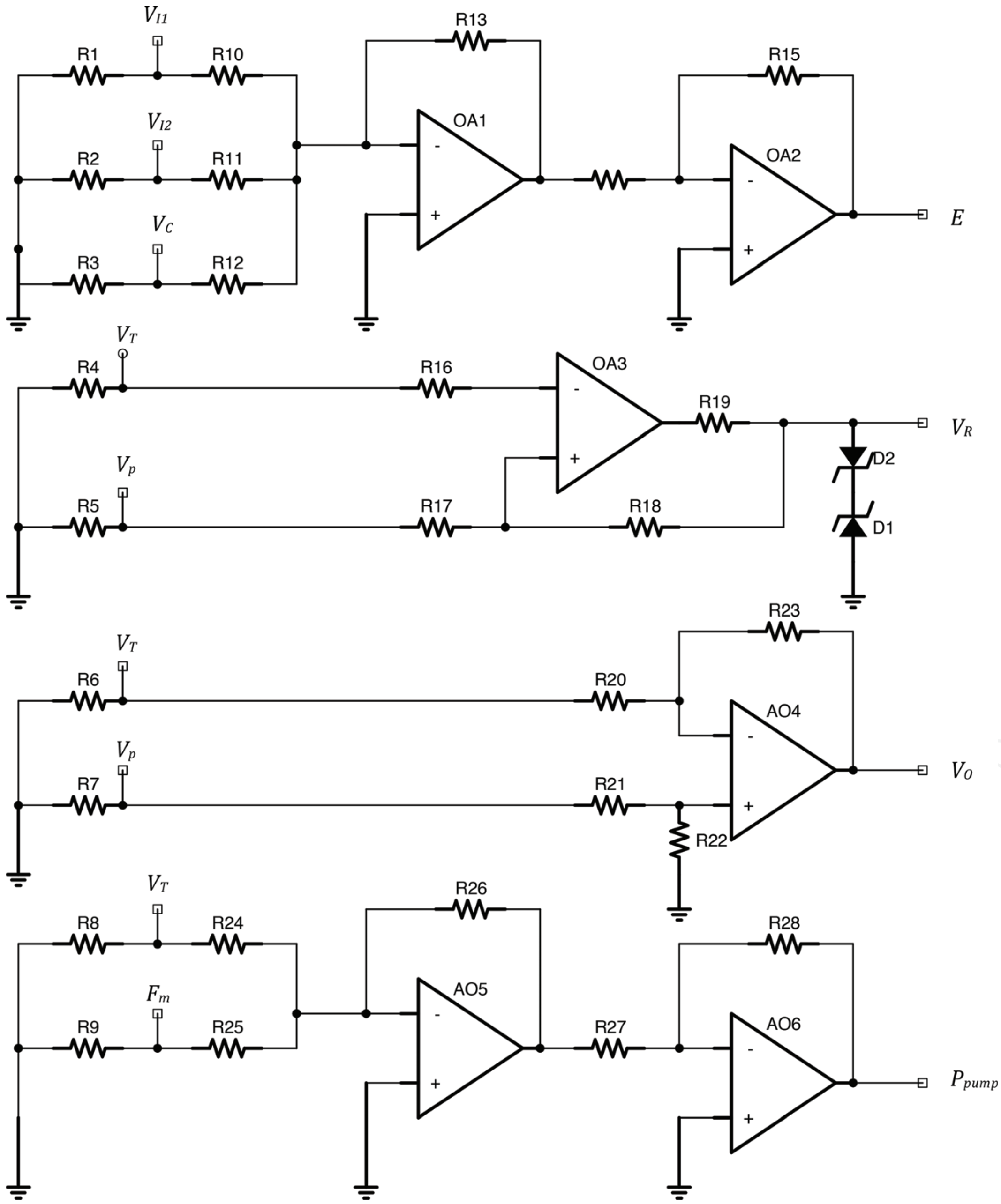

Figure 6. Electronic circuits of the threshold controller.

where V_T becomes the threshold signal.

Figure 6 shows the electronic circuits in the controller to generate E, V_R, V_0, and P_{pump} signals. The electronic components used in the controller are presented in **Table 2**.

3.2. EDFL experimental arrangement

The experimental arrangement presented in **Figure 7** consists of EDFL pumped by a laser diode (LD) from Thorlabs PL980 operating at 1560 and 977 nm, respectively. The Fabry-Perot fiber laser cavity with total length of 4.81 m is formed by an active, long EDFL of 88-cm length, and a 2.7-μm core diameter, incorporating two fiber Bragg gratings (FBG1 and FBG2) with 0.288 and 0.544-nm full widths on half-magnitude bandwidth, having, respectively, ∽100% and ∽96%

Electronic component	Value
R1–R9	100 Ω
R10–R15, R17, R19–R28	10 kΩ
R16	100 KΩ
R18	2.2 MΩ
C1, C2	100 μF
D1, D2	Zener diode
OA1 – OA6	LM741CN
I/O	Phoenix connector

Table 2. Parameters for electronic components of circuits shown in **Figure 6**.

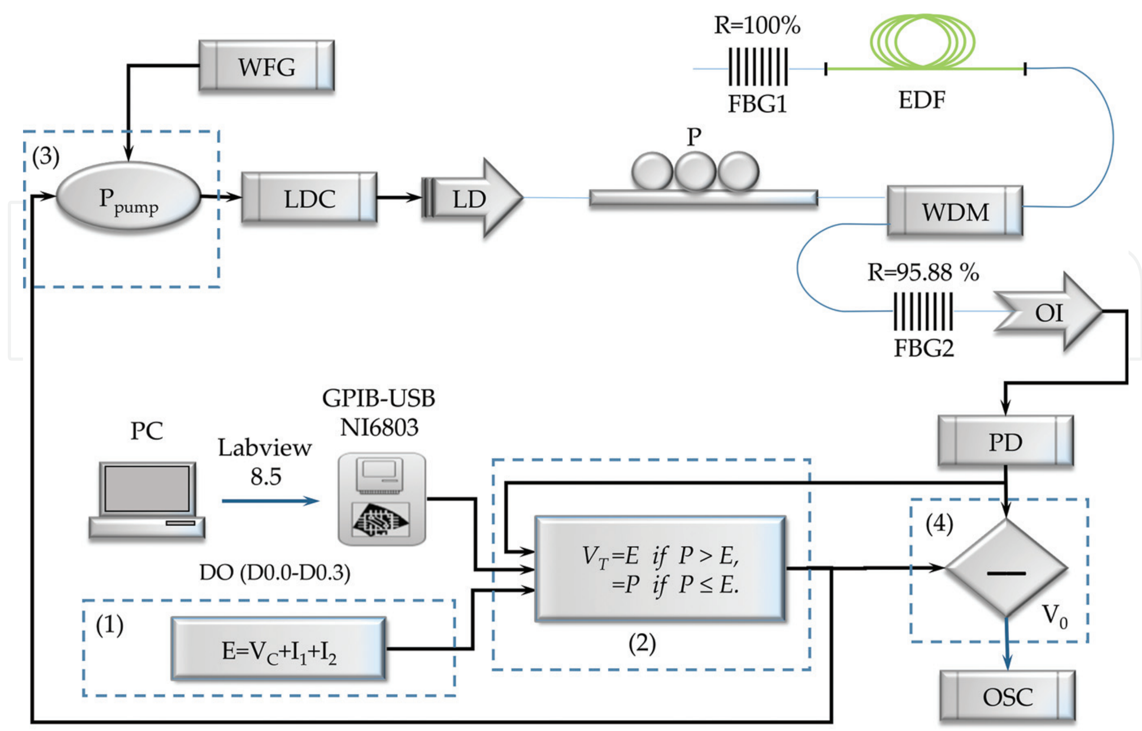

Figure 7. Experimental scheme of the optoelectronics logical gate based on EDFL.

reflectivity at the laser operating wavelength. A fiber laser formed by an erbium doped fiber (EDF) and two Bragg gratings (FBG1 and FBG2), is externally driven by the harmonic pump signal $P_{pump} = P_p[1 + A_m \sin(2\pi F_m t) + KV_T]$ (through a sum circuit CI 741) applied to a diode pump laser (LD) current via a laser diode controller (LDC) from a wave function generator (WFG). A single-mode fiber is used to connect the optical components.

The current and temperature of the LD are controlled by a laser diode controller (LDC) (Thorlabs ITC510). The 145.5-mA pump current is selected to guarantee that the laser relaxation oscillation frequency is around F_r = 30 kHz to provide a 20-mW power; which is above a 110-mA EDFL threshold current. A harmonic modulation signal $A_m \sin(2\pi F_m t)$ from wave function generator (WFG) (Tektronix AFG3102) is supplied to the diode pump current. The fiber laser output after passing through a polarization controller (P), wavelength division multiplexer (WDM), and an optical isolator (OI) is recorded with a photodiode (PD), and the electronic signal is compared with the signal generated by the threshold controller. The threshold controller with $E = V_c + I_1 + I_2$ is a summing circuit (CI 741) with dynamical control signal Vc and inputs logic signals $I_{1,2}$ controlled by a USB NI 6803, V_T is a comparator circuit between laser intensity P and threshold controller E. The logic gate output V_0 is sent back to the driver (P_{pump}) of the EDFL to change its dynamics. The signals P from the EDFL, $I_{1,2}$, V_T, and V_0 from the threshold controller are analyzed with a multichannel oscilloscope.

4. Results and discussions

4.1. Numerical results

In order to use the arrangement of the optoelectronics logic gate shown in **Figure 5**, it is necessary to determine V_c and V_{in} signals and find the required logic gates NAND or NOR.

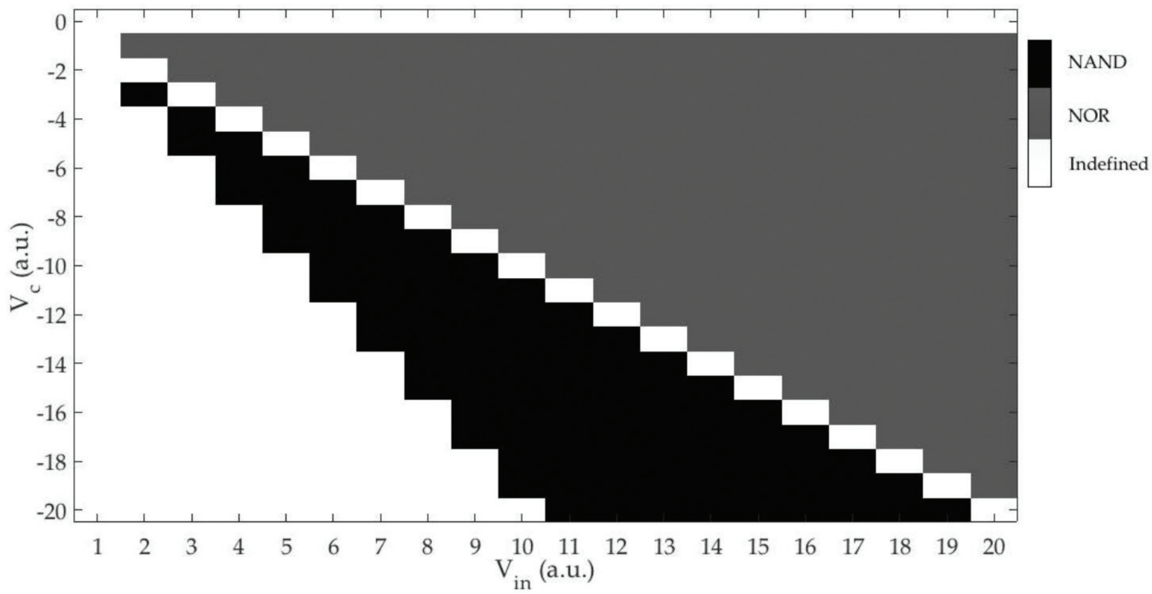

Figure 8. Diagram of values for V_c and V_{in} to determine the logic gate type, either NAND or NOR.

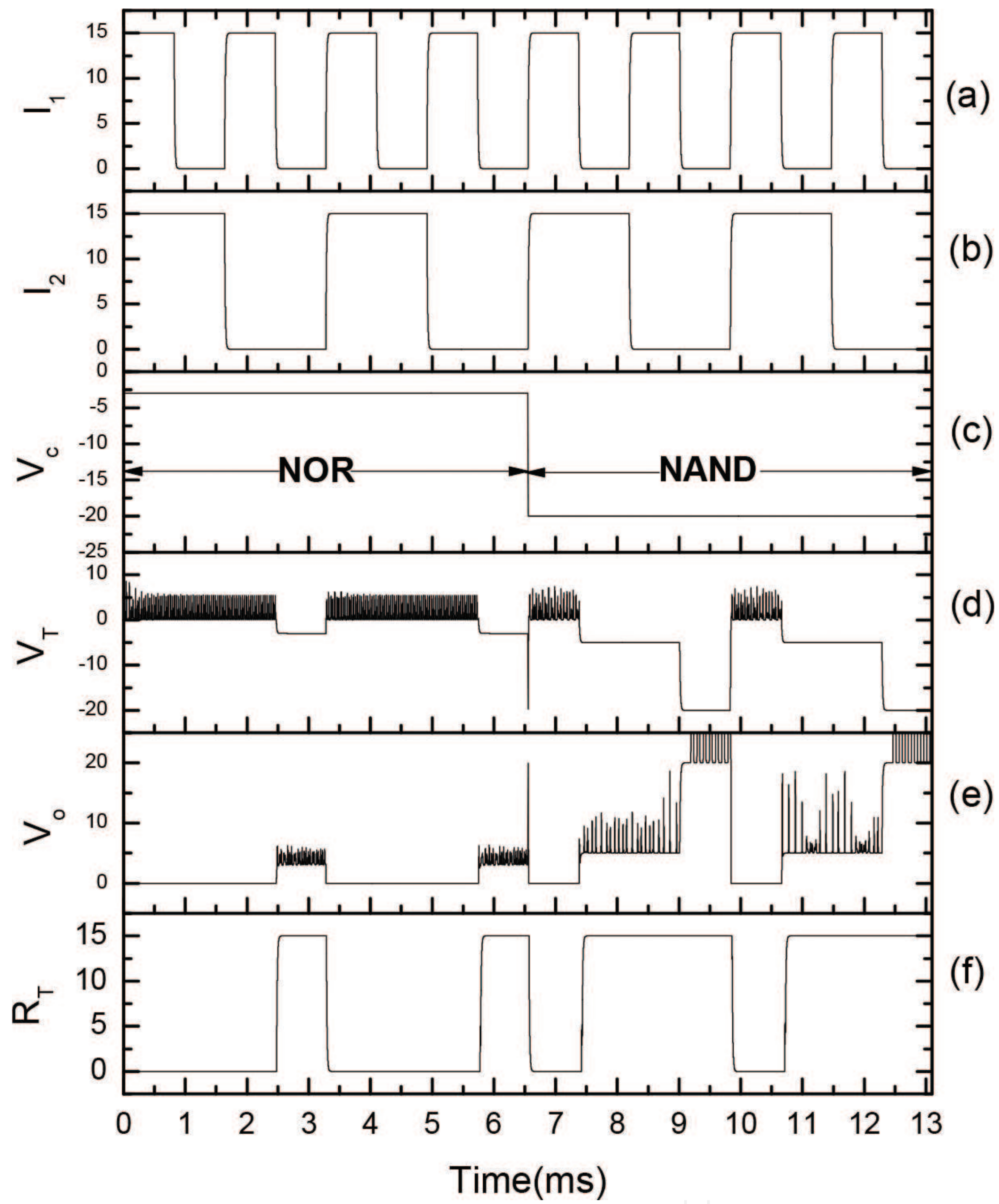

Figure 9. Numerical simulation results. (a)–(b) inputs $I_{1,2}$, (c) dynamical control signal V_c, (d) threshold controller signal V_T, (e) logic gate output V_0, and (f) recover logic output from signal V_0.

The value of V_c was gradually changed (-20 V < V_c < 2 V) and for each value of V_c the value of V_{in} was changed (2 V < V_{in} < 20 V). **Figure 8** shows the values of V_c versus V_{in} which we use to determine the logical gates NAND and NOR. If we set the parameter V_{in} = 10 V and V_c varies from -1 to -9 V, we get the NOR gate; but if V_c changes from -11 to -20 V, the NAND gate is used.

The numerical results of NOR and NAND operations of the reconfigurable dynamic logic gate Eqs. (1), (2), and (10)–(13) are shown in **Figure 9** for A_m = 1 V and F_m = 10 kHz.

For the time interval from t = 0 to 6.5 ms, we have a NOR logic gate, where the signal from V_c = – 3 V to V_{in} = 15 V produces three different combinations of the threshold controller V_T as

1. For input $I_{1,2} = (V_{in}, V_{in})$, $E = 27$ resulting in $P \leq E$ and the threshold level $V_T = P$, that yields $V_0 = 0$.
2. For input $I_{1,2} = (0, V_{in})/(V_{in}, 0)$, $E = 12$ resulting in $P \leq E$ and the threshold level $V_T = P$, that yields $V_0 = 0$.
3. For input $I_{1,2} = (0, 0)$, $E = V_c = -3$ resulting in $P > E$ and the threshold level $V_T = E$, that yields $V_0 = P - E$.

For the time interval from t = 6.5 to t = 13 ms, **Figure 9** shows a NAND logic gate, where the signal from V_c = –20 V to V_{in} = 15 V produces three different combinations of the threshold controller V_T as

1. For input $I_{1,2} = (V_{in}, V_{in})$, $E = V_c + I_1 + I_2 = V_c + 2V_{in} = 10$ resulting in $P \leq E$ and the threshold level $V_T = P$, that yields $V_0 = 0$.
2. For input $I_{1,2} = (0, V_{in})/(V_{in}, 0)$, $E = V_c + I_1 + I_2 = V_c + V_{in} = -5$ resulting in $P > E$ and the threshold level $V_T = E$, that yields $V_0 = P - E$.
3. For input $I_{1,2} = (0, 0)$, $E = V_c = -20$ resulting in $P > E$ and the threshold level $V_T = E$, that yields $V_0 = P - E$.

4.2. Experimental results

Similar to the results of the numerical simulations, a change was made in the parameters for V_c versus V_{in} to determine required NAND or NOR logic gates. **Figure 10** shows the values of V_c

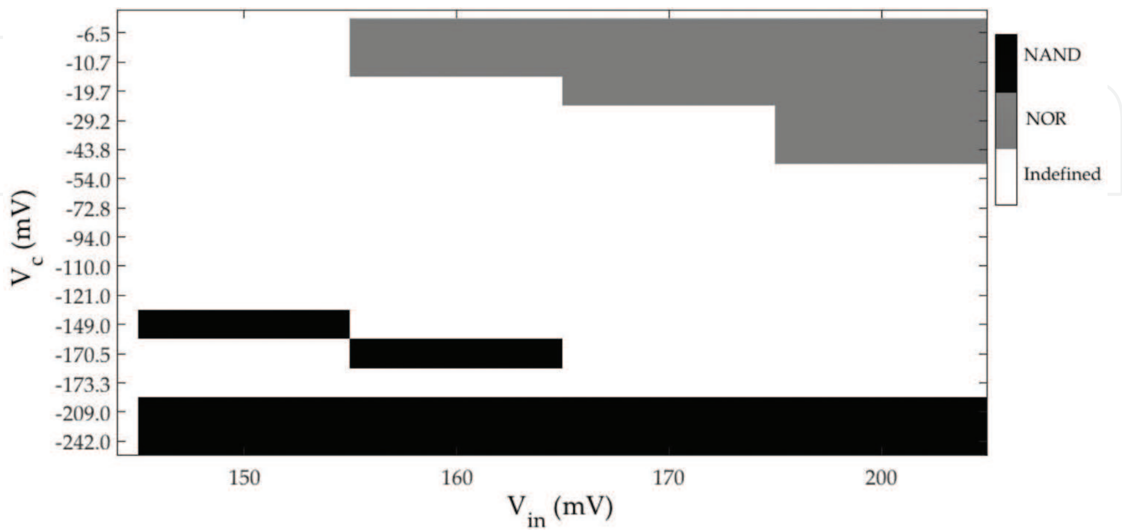

Figure 10. Diagram of values for V_c and V_{in} to determine the logic gate type, either NAND or NOR.

versus V_{in} which we use to determine the NAND and NOR logic gates. If we set the parameter V_{in} = 160 mV and changes $V_c = -10.7$ mV, we get the NOR gate, but if we change $V_c = -170.3$ mV, the NAND gate is used.

Figure 11 and **Table 3** show the experimental results of the dynamic NOR and NAND logic operations for A_m = 700 mV, F_m = 15 kHz, and V_{in} = 200 mV. The NOR gate corresponds to the time series from t = 0 ms to t = 8 ms for V_c = ©40 mV, and for the NAND gate for the time series

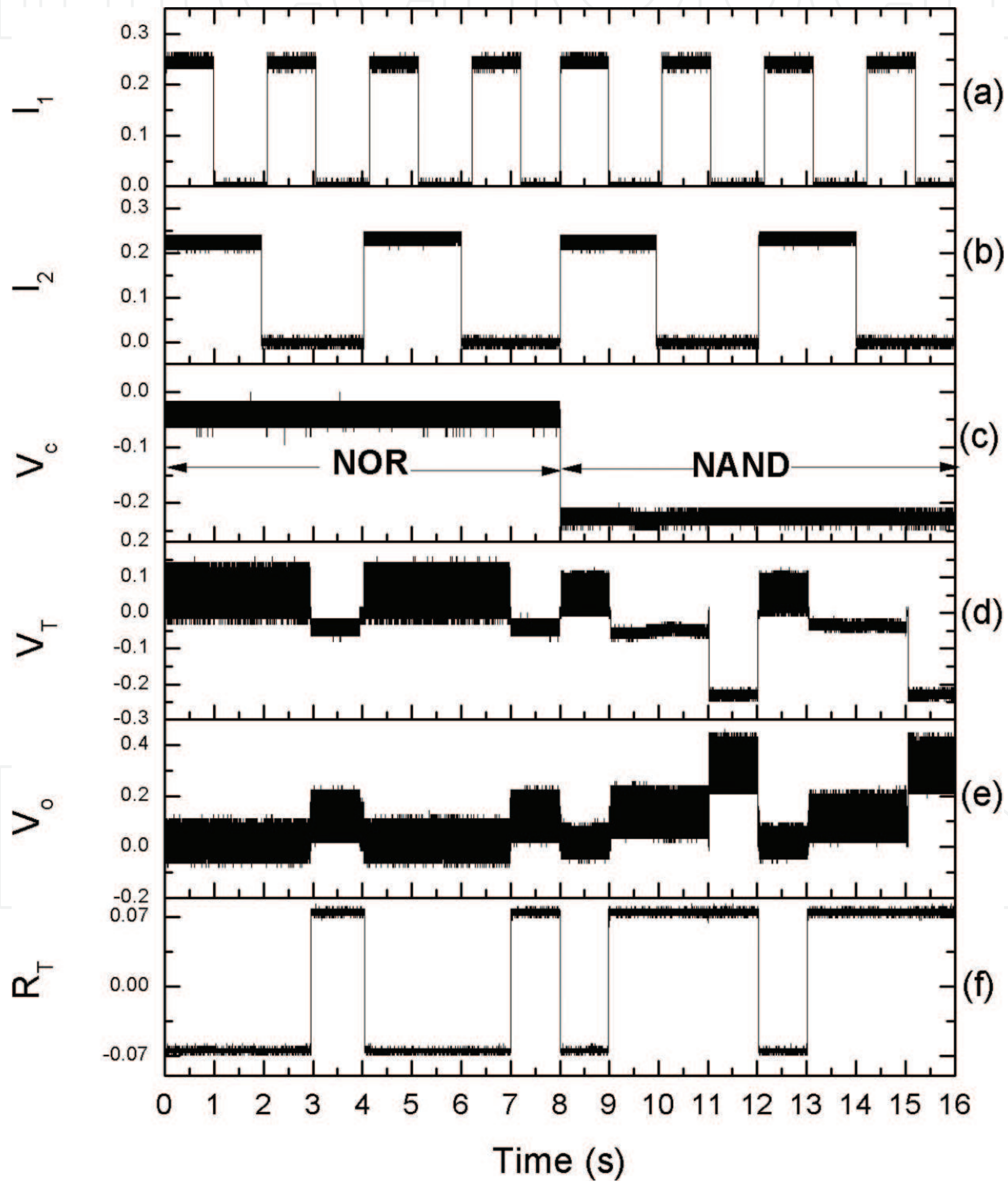

Figure 11. Experimental results. (a)–(b) inputs $I_{1,2}$, (c) dynamical control signal Vc, (d) threshold controller signal V_T, (e) logic gate output V_0, and (f) recover logic output from signal V_0.

	(I_1, I_2)	**Time**	**Threshold controller E**	V_T	V_O
	(mV)	**(ms)**	**(mV)**	**(mV)**	**(mV)**
NOR	$(\mathbf{0}, \mathbf{0})$	3–4	$E = V_c \sim -\mathbf{40}$	$E \leq P$	$V_O = P - V_T = P - E$
		7–8		$V_T = E$	
	$(V_{in}, \mathbf{0})$ *or* $(V_{in}, \mathbf{0})$	1–3	$E = V_c + V_{in} \sim \mathbf{160}$	$E > P$	$V_O = P - V_T = P - P = \mathbf{0}$
		5–7		$V_T = P$	
	(V_{in}, V_{in})	0–1	$E = V_c + \mathbf{2} * V_{in} \sim \mathbf{360}$	$E > P$	$V_O = P - V_T = P - P = \mathbf{0}$
		4–5		$V_T = P$	
NAND	$(\mathbf{0}, \mathbf{0})$	11–12	$E = V_c \tilde{} - \mathbf{220}$	$E \leq P$	$V_O = P - V_T = P - E$
		15–16		$V_T = E$	
	$(V_{in}, \mathbf{0})$ *or* $(V_{in}, \mathbf{0})$	9–11	$E = V_c + V_{in} \sim -\mathbf{20}$	$E \leq P$	$V_O = P - V_T = P - E$
		13–15		$V_T = E$	
	(V_{in}, V_{in})	8–9	$E = V_c + \mathbf{2} * V_{in} \sim \mathbf{180}$	$E > P$	$V_O = P - V_T = P - P = \mathbf{0}$
		12–13		$V_T = P$	

Table 3. Experimental data for implementation of NOR and NAND optoelectronics logical gates.

from t = 8 to t = 16 ms for V_c = −220 mV. By comparing **Figure 9** with **Figure 11**, we can see a good agreement between the numerical and experimental results.

5. Conclusions

In this chapter, we have described the implementation of an optoelectronics logic gate based on a diode-pumped EDFL. We have demonstrated good functionality of our system for NOR and NAND logic operations, taking advantage of optical chaos and a threshold controller. The system was controlled by a split signal from the threshold controller, allowing the diode pump laser to mismatch between the output threshold controller signal and the output EDFL signal. The numerical results obtained from the EDFL equations have displayed good agreement with the experimental results. We have demonstrated that the chaotic dynamic behavior of the diode-pumped EDFL and the electronic threshold controller can be successfully used to obtain NAND or NOR logic gates to be constructive bricks of different logic systems. The main contribution of the developed optoelectronics logic gate is addressed in optical computing. The proposed device is more adaptable and faster than a conventional wired hardware, since it can be implemented as an arithmetic processing unit or an optical memory RAM.

Acknowledgements

We gratefully acknowledge support and funding from the University of Guadalajara (UdeG), (R-0138/2016) under the project: Equipment of the research laboratories of the academic groups of the CULAGOS with orientation in optoelectronics, Agreement RG/019/2016-UdeG, Mexico.

Author details

Juan Hugo García-López[1]*, Rider Jaimes-Reátegui[1], Samuel Mardoqueo Afanador-Delgado[1], Ricardo Sevilla-Escoboza[1], Guillermo Huerta-Cuéllar[1], Didier López-Mancilla[1], Roger Chiu-Zarate[1], Carlos Eduardo Castañeda-Hernández[1] and Alexander Nikolaevich Pisarchik[2]

*Address all correspondence to: jhugo.garcia@academicos.udg.mx

1 Department of Exact Sciences and Technology, University of Guadalajara, Lagos de Moreno, Jalisco, Mexico

2 Center for Biomedical Technology, Technical University of Madrid, Madrid, Spain

References

[1] Digonnet M, Snitzer E. Rare earth doped fiber lasers and ampliers. In: Digonnet MJF, editor. Marcel Dekker, Chapter 5; 1993. ISBN-13: 978-0824704582, ISBN-10: 0824704584

[2] Luo LG, Chu PL. Optical secure communications with chaotic erbium-doped fiber lasers. Journal of the Optical Society of America B. 1998;**15**:2524-2530. DOI: https://doi.org/10.1364/JOSAB.1-5.002524

[3] Saucedo-Solorio JM, Pisarchik AN, Kiŕyanov A V, Aboites V. Generalized multistability in a fiber laser with modulated losses. Journal of the Optical Society of America B. 2003;**20**:490-496. DOI: https://doi.org/10.1364/JOSAB.20.000490

[4] Pisarchik AN, Barmenkov YuO, Kiryanov AV. Experimental characterization of the bifurcation structure in an erbium-doped fiber laser with pump modulation. IEEE Journal Quantum Electronics. 2003;**39**:1567-1571. DOI: 10.1109/JQE.2003.819559

[5] Pisarchik AN, Barmenkov Yu O, Kiryanov AV. Experimental demonstration of attractor annihilation in a multistable fiber laser. Physical Review E. 2003;**68**. DOI: https://doi.org/10.1103/PhysRevE.68.066211

[6] Reátegui RJ, Kiryanov AV, Pisarchik AN, Barmenkov Yu O, Ilichev NN. Experimental study and modelling of coexisting attractors and bifurcations in an erbium-doped fiber laser with diode-pump modulation. Laser Physics. 2004;**14**:1277

[7] Pisarchik AN, Kiryanov AV, Barmenkov Yu O, Jaimes-Reategui R. Dynamics of an erbium-doped fiber laser with pump modulation: theory and experiment. Journal of the Optical Society of America B. 2005;**22**:2107. DOI: https://doi.org/10.1364/JOSAB.22.002107

[8] Huerta-Cuellar G, Pisarchik AN, Barmenkov Yu O. Experimental characterization of hopping dynamics in a multistable fiber laser. Physical Review E. 2008;**78**. DOI: https://doi.org/10.1103/PhysRevE.78.035202

[9] Pisarchik AN, Jaimes-Reátegui R. Control of basins of attraction in a multistable fiber laser. Physics Letters A. 2009;**374**:228. DOI: https://doi.org/10.1016/j.physleta.2009.10.061

[10] Huerta-Cuellar G, Pisarchik AN, Kiryanov AV, Barmenkov Yu O, Del Valle Hernández J. Prebifurcation noise amplification in a fiber laser. Physical Review E. 2009;**79**:1. DOI: https://doi.org/10.1103/PhysRevE.79.036204

[11] Pisarchik AN, Jaimes-Reátegui R, Sevilla-Escoboza R, Huerta-Cuellar G, Taki M. Rogue waves in a multiestable system. Physical Review Letters. 2011;**107**:1. DOI: https://doi.org/10.1103/PhysRevLett.107.274101

[12] Pisarchik AN, Jaimes-Reátegui R, Sevilla-Escoboza JR, Huerta-Cuellar G. Multistable intermittency and extreme pulses in a fiber laser. Physical Review E. 2012;**86**:1. DOI: https://doi.org/10.1103/PhysRevE.86.056219

[13] Ditto WL, Murali K, Sinha S. Chaos computing: Ideas and implementations. Philosophical Transactions of the Royal Society A. 2008;**366**:653-664. DOI: 10.1098/rsta.2007.2116

[14] Sinha S, Ditto W L. Dynamics based computation. Physical Review Letters. 1998;**81**;2156. DOI: https://doi.org/10.1103/PhysRevLett.81.2156

[15] Sinha S, Munakata T, Ditto WL. Flexible parallel implementation of logic gates using chaotic elements. Physical Review E. 2002;**65**:1. DOI: https://doi.org/10.1103-/PhysRevE.65.036216

[16] Sinha S, Ditto WL. Computing with distributed chaos. Physical Review E. 1999;**60**:363. DOI: https://doi.org/10.1103/PhysRevE.60.363

[17] Murali K, Sinha S, Ditto W L. Construction of a reconfigurable dynamic logic cell. Pramana. 2005;**64**:433. DOI https://doi.org/10.1007/BF02704569

[18] Murali K, Sinha S, Ditto WL. Implementation of a NOR gate by a chaotic chua's circuit. International Journal of Bifurcation and Chaos. 2003;**13**:2669. DOI: https://doi.org/10.1142-/S0218127403008053

[19] Taubes G. Computer design meets Darwin. Science. 1997;**277**:1931. DOI: https://doi.org/10.1126/science.277.5334.1931

[20] Ditto W, Sinha S, Murali K. US Patent Number 07096347. 2006

[21] Prusha BS, Lindner J F. Nonlinearity and computation: implementing logic as a nonlinear dynamical system. Physics Letters A. 1999;**263**:105. DOI: https://doi.org/10.1016/S0375-9601(99)00665-9

[22] Cafagna D, Grassi G. Dynamic behaviour and route to chaos in experimental boost converter. International Symposium on Signals, Circuits and Systems. 2005;**2**:745. DOI: 10.1109 /ISSCS.2005.1511348

[23] Chlouverakis KE, Adams MJ. Optoelectronic realisation of NOR logic gate using chaotic two-section lasers. Electronics Letters. 2005;**41**:359. DOI: http://dx.doi.org/10.1049/el:20058026

[24] Jahed-Motlagh MR, Kia B, Ditto WL, Sinha S. Fault tolerance and detection in chaotic computers. International Journal of Bifurcation and Chaos. 2007;**17**:1955-1968. DOI: https://doi.org/10.1142/S0218127407018142

[25] Murali K, Miliotis A, Ditto W L, Sinha S. Logic from circuit elements that exploit nonlinearity in the presence of a moise floor. Physics Letters A. 2009;**373**:1346. DOI: https://doi.org/10.1016/j.physleta.2009.02.026

[26] Ditto WL, Miliotis A, Murali K, Sinha S. The chaos computing paradigm. In: HeinzGeorg Schuster, editor. Reviews of Nonlinear Dynamics and Complexity. Vol. 3. Weinheim: WILEY-VCH Verlag GmbH & Co. KGaA; 2010. p. 1-35. ISBN: 978-3-527-40945-7

[27] Jaimes-Reategui R, Afanador-Delgado SM, Sevilla-Escoboza R, Huerta-Cuellar G, Hugo G-LJ, Lopez-Mancilla D, Castañeda-Hernandez C, Pisarchik AN. Optoelectronic flexible logic gate based on a fiber laser. The European Physical Journal Special Topics. 2014;**223**: 2837-2846. DOI: 10.1140/epjst/e2014-02297-4

[28] García-López JH, Jaimes-Reátegui R, Afanador-Delgado SM, Sevilla-Escoboza R, Huerta-Cuellar G, Casillas-Rodríguez FJ, López-Mancilla D, Pisarchik AN. Optoelectronic flexible logic-gate using a chaotic erbium doped fiber laser, experimental results. In: *Latin America Optics and Photonics Conference*. OSA Technical Digest (online) (Optical Society of America, 2014), paper LTu4A.36. DOI: https://doi.org/10.1364/LAOP.2014.LTu4A.36

[29] Jaimes-Reátegui R. Dynamic of Complex System with Parametric Modulation Duffing Oscillators and a Fiber Laser (Thesis). Leon, Guanajuato, Mexico: Center for Optical Research; 2004

[30] Afanador Delgado SM. Implementación opto-electrónica de una compuerta lógica dinámicamente configurable usando un láser de fibra (thesis). Lagos de Moreno, Jalisco, Mexico: CULagos, University of Guadalajara; 2014